




Article

Experimental Study and Mathematical Modeling of the Processes Occurring in ZrN Coating/Silumin Substrate Systems under Pulsed Electron Beam Irradiation

Nikolay N. Koval ^{1,*}, Tamara V. Koval ², Olga V. Krysinina ¹, Yurii F. Ivanov ¹, Anton D. Teresov ¹, Pavel V. Moskvina ¹, My Kim An Tran ³, Nikita A. Prokopenko ¹ and Elizaveta A. Petrikova ¹

- ¹ Institute of High Current Electronics SB RAS, 2/3 Akademicheskoy Avenue, 634055 Tomsk, Russia; krysinina@opee.hcei.tsc.ru (O.V.K.); yufi55@mail.ru (Y.F.I.); tad514@yandex.ru (A.D.T.); pavmoskvina@mail.ru (P.V.M.); nick08_phantom@mail.ru (N.A.P.); elizmarkova@yahoo.com (E.A.P.)
- ² School of Computer Science and Robotics, Tomsk Polytechnic University, 30 Lenina Avenue, 634059 Tomsk, Russia; tvkoval@mail.ru
- ³ Faculty of Mathematics and Statistics, Ton Duc Thang University, 19 Nguyen Huu Tho Street, Ho Chi Minh City 756000, Vietnam; tranmykiman@tdtu.edu.vn
- * Correspondence: koval@opee.hcei.tsc.ru; Tel.: +7-3822492792



Citation: Koval, N.N.; Koval, T.V.; Krysinina, O.V.; Ivanov, Y.F.; Teresov, A.D.; Moskvina, P.V.; Tran, M.K.A.; Prokopenko, N.A.; Petrikova, E.A. Experimental Study and Mathematical Modeling of the Processes Occurring in ZrN Coating/Silumin Substrate Systems under Pulsed Electron Beam Irradiation. *Coatings* **2021**, *11*, 1461. <https://doi.org/10.3390/coatings11121461>

Academic Editor: Emerson Coy

Received: 29 October 2021

Accepted: 25 November 2021

Published: 28 November 2021

Publisher's Note: MDPI stays neutral with regard to jurisdictional claims in published maps and institutional affiliations.



Copyright: © 2021 by the authors. Licensee MDPI, Basel, Switzerland. This article is an open access article distributed under the terms and conditions of the Creative Commons Attribution (CC BY) license (<https://creativecommons.org/licenses/by/4.0/>).

Abstract: This paper presents a study of a combined modification of silumin, which included deposition of a ZrN coating on a silumin substrate and subsequent treatment of the coating/substrate system with a submillisecond pulsed electron beam. The local temperature on the samples in the electron-beam-affected zone and the thickness of the melt zone were measured experimentally and calculated using a theoretical model. The Stefan problem was solved numerically for the fast heating of bare and ZrN-coated silumin under intense electron beam irradiation. Time variations of the temperature field, the position of the crystallization front, and the speed of the front movement have been calculated. It was found that when the coating thickness was increased from 0.5 to 2 μm , the surface temperature of the samples increased from 760 to 1070 $^{\circ}\text{C}$, the rise rate of the surface temperature increased from 6×10^7 to 9×10^7 K/s, and the melt depth was no more than 57 μm . The speed of the melt front during the pulse was 3×10^5 $\mu\text{m/s}$. Good agreement was observed between the experimental and theoretical values of the temperature characteristics and melt zone thickness.

Keywords: pulsed electron beam; electron beam treatment; vacuum arc deposition; ZrN coating; silumin substrate; coating/substrate system; temperature measurement; mathematical modeling; crystallization rate; melt depth

1. Introduction

To control the properties of the surface layer of machine parts and mechanisms, various approaches are used that involve changing the elemental composition of the surface layer by ion implantation [1,2], ion mixing [3], and diffusion of alloying elements from gaseous [4,5], liquid [6,7] or solid [8,9] states. Complex alloying is also widely used, such as alloying of steels with metal atoms for further (or simultaneous) saturation of the surface layer with non-metallic atoms (nitrogen, carbon, boron) [10]. Examples of surface alloying are electro-explosive alloying [11,12] followed by pulsed electron beam treatment [13–15] and treatment of targets with pre-deposited films of alloying elements (aluminum, titanium, nickel, chromium, etc.) by compression plasma flows [16–19]. Such treatment produces remelted layers of a depth of up to 30 μm and a heat-affected zone of depth about 200 μm .

One of the most promising combined methods that are of interest to scientific researchers is coating deposition with subsequent electron beam treatment of the coating/substrate system [20–22]. It should be noted that this method, depending on the input energy density and the coating and substrate compositions, allows one to produce surface

alloys of different compositions with the alloyed layer thickness from 0.1 to 100 μm [21–23] or to fuse single-layer hard coatings into lower melting point substrates to produce highly adhesive layers with enhanced properties [24,25].

These combined methods are particularly relevant for the modification of light aluminum alloys (including silumins) the industrial use of which is limited by their low tribological and strength characteristics [26,27]. The nonequilibrium structure-phase states are formed in the surface layer of materials under electron beam irradiation on the microsecond and submillisecond time scales due to ultra-high rates of heating (up to 10^6 deg/s) of a thin surface layer of the material (1–10 μm) to melting temperatures and due to very high temperature gradients (up to 10^7 – 10^8 deg/m), which provide cooling of the surface layer by heat transfer to the bulk material at a rate of 10^4 – 10^6 deg/s.

The temperature of the material in the electron beam treatment zone and the rate of its variation, as well as the rate of heating and cooling of the material, are the main characteristics that affect the formation of the modified layer structure. In turn, the temperature characteristics are affected by the energy of the beam electrons arriving at the substrate (energy density in a pulse), the properties of both the coating and the substrate materials (thermal conductivity, melting point, etc.), the thickness of the irradiated coating, and the method and rate of cooling of the coating/substrate system.

Different methods for treating materials and producing coatings can lead to different impurity contents and to the presence of point defects, which affect the thermal and mechanical properties of the substrate and coating materials and can be a source of scatter in their characteristics [28–31]. The characteristics of the coating material are also affected by its thickness. Therefore, to solve the thermal problem of the action of intense energy fluxes on a coating/substrate system, it is important to combine modeling and measuring of the surface temperature. This makes it possible to refine the thermophysical parameters of the materials to predict the dynamics of the temperature fields and, accordingly, the structure of the modified layer.

The aim of this work was to perform a combined modification of a eutectic silumin, including deposition of a ZrN coating on a silumin substrate and treatment of the coating/substrate system with a pulsed electron beam. The local temperature in the beam-affected zone was measured and numerically calculated. A theoretical modeling was performed to analyze the processes responsible for the modification of the coating/substrate system irradiated with an electron beam under given conditions. These investigations provide a basis for increasing predictably the service life of silumin products, which could significantly expand the area of their use.

2. Materials and Methods

The test ZrN coatings of thickness 0.5, 1, and 2 μm were deposited on the substrates by the vacuum-arc method on the QUINTA specialized ion-plasma installation, in the mode with magnetic filtration of the plasma flow [32,33] (Institute of High Current Electronics, Tomsk, Russia). The coating deposition was carried out at the following parameters: arc evaporator current $I_d = 90$ A, Ar/N₂ content ratio = 1/1, working pressure of the gas mixture $p = 0.3$ Pa, negative pulsed substrate bias voltage $U_b = 150$ V, and pulse duty factor $\gamma = 85\%$. The growth rate of the coatings was 2.7 $\mu\text{m}/\text{h}$. The deposition time, chosen in accordance with the growth rate and the required coating thickness, was 11, 22, and 44 min for coatings of thickness 0.5, 1, and 2 μm , respectively. The deposition parameters were chosen proceeding from a previous study [33]. However, the discharge current of the evaporator was chosen such that the temperature of the low-melting silumin samples during deposition was not over 350 °C.

The substrates were samples of AK12 (eutectic) silumin (10–13% Si + 84.3–90% Al) $15 \times 15 \times 4$ mm³ in size.

Electron beam irradiation of the samples and measurement of their surface temperature were performed using the SOLO electrophysical vacuum setup [34]. It was designed to study the effect of concentrated energy fluxes on materials and to perform surface

modification of metal and cermet products in order to improve their operational properties. The main component of the setup is a pulsed electron source of the same name 1 (Figure 1) with a plasma cathode produced by a low-pressure arc discharge [35,36], developed at the Institute of High Current Electronics (Tomsk, Russia). It generates an electron beam of energy 5–25 keV, current 20–300 A, and pulse duration 20–200 μs at a pulse repetition rate of 0.3–20 s^{-1} . The energy density distribution over the beam cross section has a Gaussian profile with a maximum of up to 100 J/cm^2 , and the beam diameter in the target area is about 3 cm. The distribution profile can be controlled by changing the configuration and magnitude of the magnetic field of solenoids 2 and 3 (see Figure 1) in the range between 0.01 and 0.1 T. Thus, the beam uniformity could be no less than $\pm 15\%$ of the average current density over about 7 cm^2 in the treatment zone. The plasma electron source was powered by specialized power supplies 5, 6, and 7, and the diagnostics were performed with oscilloscope 8. Sample 10 with thermocouple 11 was fixed on movable manipulator table 9. The thermocouple signal was fed to oscilloscope 8 through normalizing converter 12.

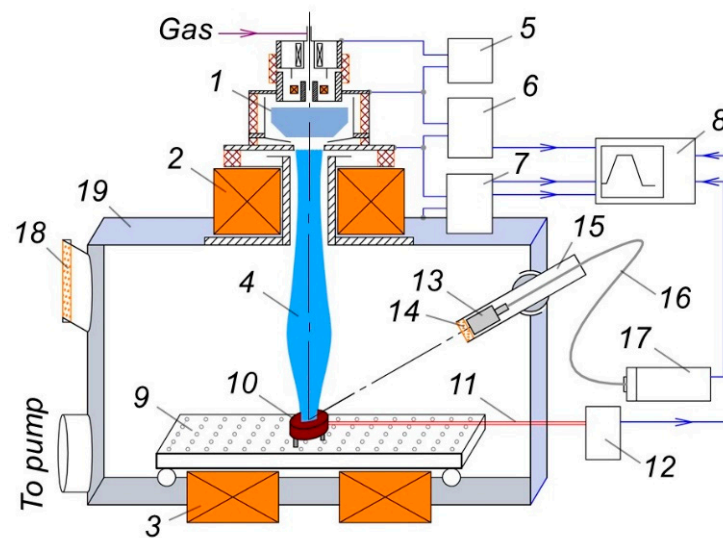


Figure 1. Schematic diagram of the experimental setup: 1—SOLO electron source, 2, 3—magnetic coils, 4—electron beam, 5—auxiliary discharge power supply, 6—plasma cathode discharge power supply, 7—accelerating voltage power supply, 8—oscilloscope, 9—manipulator table, 10—thermally insulated sample, 11—thermocouple, 12—normalizing converter, 13—lens, 14—quartz glass, 15—rotary joint, 16—fiber-optic cable, 17—high speed pyrometer, 18—viewing window, and 19—vacuum chamber.

The electron source used is capable of working with various inert and reaction gases. In the experiments performed, argon was fed into the source at a leakage rate of 0.03–0.04 $\text{Pa} \cdot \text{m}^3/\text{s}$, which provided a constant pressure of 0.1 Pa in the vacuum chamber.

The local surface temperature of the samples was measured with a high-speed infrared pyrometer (Kleiber KGA 740-LO) 17 (see Figure 1). It operates in the spectral range 2.0–2.2 μm , provides a response time of 6 μs , and can measure temperatures in the range of 300–2300 $^{\circ}\text{C}$. The thermal radiation from the sample passed through quartz glass 14 and LVO 25 lens 13 mounted on vacuum-tight rotary joint 15. The lens was connected to the pyrometer using flexible fiber-optic cable 16. The measurement area on the sample was an ellipse with dimensions of $\approx 4 \times 8 \text{ mm}^2$. The device converts the measured temperature into a voltage (0–10 V) according to a linear law. The signal voltage, together with the discharge current of the plasma cathode of the electron source, I_d , the current in the acceleration gap, I_g , and the accelerating voltage, U_g , were recorded with oscilloscope 8. The beam treatment process could be visually observed through lead glass viewing window 18 of vacuum chamber 19.

When performing measurements with any brightness temperature pyrometer, to which the used model belongs, it is necessary to set the emissivity of the object surface. To determine it, the (thermally insulated) sample was smoothly heated to 500 °C by an electron beam with gentle parameters (beam energy density $E_S = 0.5 \text{ J/cm}^2$, pulse duration $\tau = 50 \text{ }\mu\text{s}$, pulse repetition rate $f = 8 \text{ Hz}$, and accelerating voltage $U_g = 13 \text{ kV}$) in argon at a pressure of 0.1 Pa. This approach made it possible to heat the sample in bulk without changing its surface state. Then, when the sample was cooling, the emissivity was set on the pyrometer so that close readings of the pyrometer and K-type thermocouple 11, made of chromel and alumel wires 0.3 mm in diameter, could be achieved. After that, based on contact temperature measurements, a calibration straight line was constructed, which represented the final dependence of the output voltage of the pyrometer on the local surface temperature for the given sample. The procedure for constructing a calibration straight line was repeated after treating the sample with working beam pulses. This was made to evaluate the possible measurement error caused by the change in state of the irradiated sample surface and, as a consequence, by the change in surface emissivity.

The electron beam treatment of the silumin substrates was carried out according to the modes presented in Table 1. At the initial stage, all silumin samples were mechanically ground using abrasive paper. Then, the samples were preliminarily treated with an electron beam (mode 1) to degas and polish the surface and to remove surface impurities. After coating deposition, the ZrN coating/silumin substrate system was treated with an electron beam according to the main mode (mode 2).

Table 1. Modes of electron beam treatment of the samples.

Sample No.	ZrN Coating Thickness, μm	Preliminary Treatment Mode (Mode 1)	Main Treatment Mode (Mode 2)
1	0	$E_S = 30 \text{ J/cm}^2$, $\tau = 200 \text{ }\mu\text{s}$,	-
2	0.5 ± 0.08	$N = 10 \text{ pulses}$, $f = 0.3 \text{ Hz}$,	$E_S = 25 \text{ J/cm}^2$, $\tau = 150 \text{ }\mu\text{s}$,
3	1 ± 0.11	$U_g = 13 \text{ kV}$	$N = 5 \text{ pulses}$, $f = 0.3 \text{ Hz}$,
4	2 ± 0.14		$U_g = 13 \text{ kV}$

The structure of the modified layer before and after combined electron-ion-plasma treatment (coating deposition and electron beam irradiation) was examined using optical microscopy ($\mu\text{Vizo-MET-221}$ metallographic microvisor device, LOMO, St. Petersburg, Russia) and scanning electron microscopy (Philips SEM-515 device with EDAX ECON IV microanalyzer, Philips, Amsterdam, Netherlands).

3. Mathematical Model and Numerical Calculations

The dynamics of the temperature field in a sample irradiated with an intense electron beam is described by the heat transfer equation with proper boundary conditions and initial conditions, taking into account the assumptions of the mathematical model. In the mathematical formulation of the problem, it can be assumed that an electron beam energy of <20 keV acts as a surface energy source and that the thermal processes can be considered in a one-dimensional approximation with an irradiation pulse duration of 150 μs .

The heating of the sample is described by the equations

$$\rho c \frac{\partial T}{\partial t} = \frac{\partial}{\partial x} \left(\lambda \frac{\partial T}{\partial x} \right), \quad (1)$$

$$-\lambda \frac{\partial T(t, 0)}{\partial x} = p(t), \quad \frac{\partial T(t, l)}{\partial x} = 0, \quad T(0, x) = T_0,$$

where c is the specific heat capacity of the sample material, ρ is its density, λ is its thermal conductivity, $p(t) = U(t)j(t)$ is the power density of the electron beam, $U(t)$ is the accelerating voltage, $j(t)$ is the beam current density, and l is the length of the sample.

The mathematical model accounts for the existence of a two-phase region, which is characterized by the average volume fraction of the liquid phase, θ , in the solid/liquid system [37,38]. The phase transition occurs in the temperature range from $T_{tr} - \Delta T/2$ to $T_{tr} + \Delta T/2$ (T_{tr} is the phase transition temperature) for which the material phase is modeled by a smoothed function θ varying from 1 to 0. The effective thermal conductivity of the solid(s)/liquid(l) system, λ , is related to the conductivity of the solid; λ_s , and the conductivity of the liquid, λ_l , as

$$\lambda = (1 - \theta)\lambda_s + \theta\lambda_l$$

The material density in the two-phase region and the heat capacity are assumed to be constant. The latent heat of melting, L , involved in the phase transition is included in the specific heat as an additional term:

$$c = c_s + \frac{L}{\Delta T}$$

The phase transition between liquid and solid is described in a similar way. The system of Equation (1) was solved numerically with an implicit difference scheme, which was previously used in [39,40]. This scheme, when implemented using the MATLAB software package, makes it possible to obtain satisfactory agreement of numerical calculations with experimental measurements. Table 2 shows the thermophysical parameters of the silumin [28–31] and the coating [30,31] used for numerical calculations. Regarding the experimental conditions, evaporation could be considered negligible (the evaporation temperature of silumin is 2493 °C). The dependences of the coating's heat capacity and thermal conductivity have been found by numerical experiments performed for the calculated temperature being in agreement with the measured one. The lower the thickness of the coating, the higher the rate of change in the thermal conductivity of the coating with temperature. This is due to the more rapid destruction of the coating structure under electron beam irradiation and the change in the surface layer composition as a result of the melting of the base.

Table 2. Thermal and physical characteristics of the substrate and coating materials.

Symbol/ Dimension	Value	Description
Silumin		
$c_{s,l}$, J kg ⁻¹ K ⁻¹	1177	Heat capacity
$\rho_{s,l}$, kg m ⁻³	2600	Density
λ_s , W m ⁻¹ K ⁻¹	130 (on heating)120 (on cooling)	Thermal conductivity of solid
λ_l , W m ⁻¹ K ⁻¹	$60 + 0.024(T - T_{tr} - \Delta T/2)$	Thermal conductivity of liquid ($T_{tr} + \Delta T/2 \leq T < 1400$ °C)
$T_{tr}/\Delta T$, °C	580/12	Phase transition temperature/interval for melting
$T_{tr}/\Delta T$, °C	562/24	Phase transition temperature/interval for crystallization
L , kJ kg ⁻¹	385	Latent heat of melting
ZrN coating		
c , J kg ⁻¹ K ⁻¹	$-1926(T + 300)^{-0.07585} + 1626 + a(h_{ZrN})$, $a(h_{ZrN} = 0.5 \mu\text{m}) = 0$, $a(1) = 24, a(2) = 124$	Heat capacity
ρ , kg m ⁻³	7090	Density
λ , W m ⁻¹ K ⁻¹	$-4658(T + 300)^{-0.9633} + 50.36 + b(h_{ZrN})$, $b(h_{ZrN} = 0.5 \mu\text{m}) = 0$, $b(1) = -20, b(2) = -25$	Thermal conductivity
T_m , °C	2280	Melting point
L , kJ kg ⁻¹	371	Latent heat of melting

4. Results and Discussions

Preliminary electron beam treatment caused surface melting of the silumin (Figure 2a) to a depth of 40 μm (Figure 3a, the molten layer is indicated by the arrow; Table 3). It was found that pulsed electron beam irradiation (25 J/cm^2 , 150 μs , 5 pulses, 0.3 Hz) of the ZrN coating/silumin substrate system with a ZrN-coating thickness of 0.5–2 μm resulted in a partial destruction of the coating, melting of the surface layer of the substrate, and emergence of the melt on the surface of the coating, which indicated that the coating was fused to the substrate (Figure 2b–d).

Examination of transverse sections of the coated silumin after electron beam treatment revealed, as in the case of the bare silumin, a melt zone, where melting of all phases of the substrate was observed (see Figure 3). In the melting zone of the samples with coatings of different thicknesses, immersion of the coating fragments into the bulk substrate to a depth of 45 μm was observed (see Figure 3; the coating fragments in the bulk substrate are indicated by white arrows). The thickness of the melting zone increased with the thickness of the ZrN coating. For the silumin subjected to preliminary electron beam treatment (sample 1), the thickness of the melting zone, evaluated from optical and SEM images of thin transverse sections, was 30–40 μm . For the samples subjected to combined treatment (samples 2 through 4), the thickness of the melting zone increased from 30–45 to 40–55 μm when the thickness of the ZrN coating was increased from 0.5 to 2 μm . The maximum immersion depth of the coating fragments also increased with coating thickness. This was associated with an increase in the gravity of the coating parts immersed in the melt upon electron beam irradiation and an increase in the thickness of the melting zone with increasing local temperature in the treatment zone.

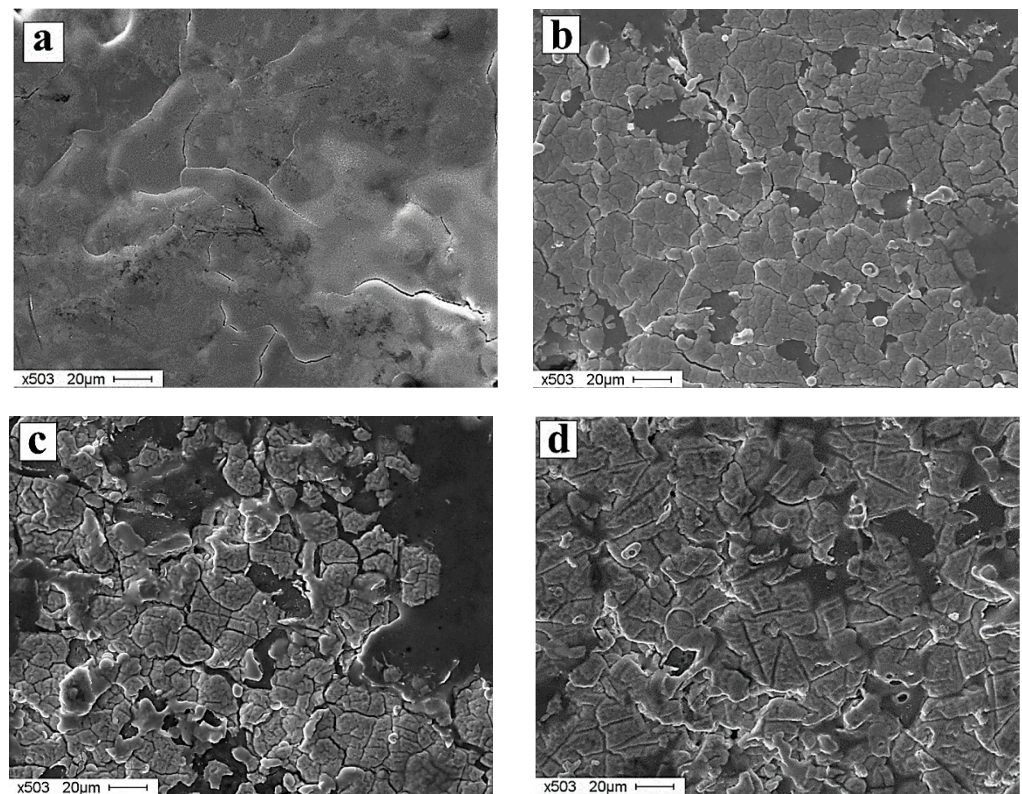


Figure 2. SEM images of the surface structure of the bare and ZrN-coated silumin after electron beam treatment: sample 1 (no coating) (a), sample 2 ($h_{\text{ZrN}} = 0.5 \mu\text{m}$) (b), sample 3 ($h_{\text{ZrN}} = 1 \mu\text{m}$) (c), and sample 4 ($h_{\text{ZrN}} = 2 \mu\text{m}$) (d).

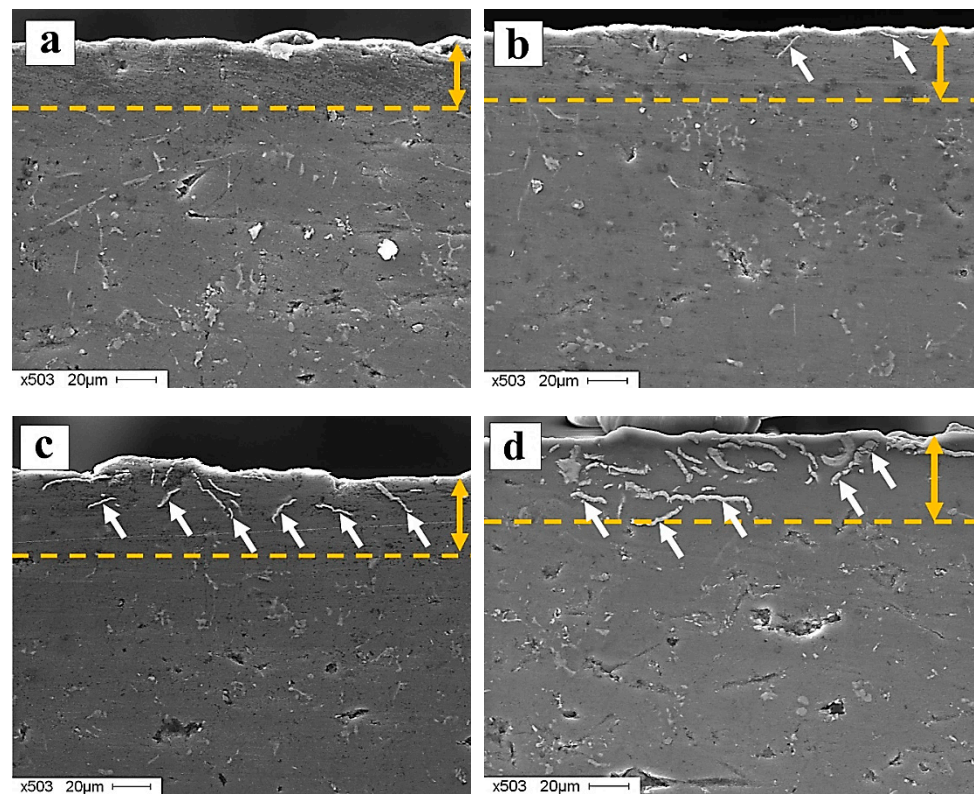


Figure 3. SEM images of the surface structure of silumin without and with a ZrN coating after electron beam treatment: sample 1 (no coating) (a), sample 2 ($h_{\text{ZrN}} = 0.5 \mu\text{m}$) (b), sample 3 ($h_{\text{ZrN}} = 1 \mu\text{m}$) (c), and sample 4 ($h_{\text{ZrN}} = 2 \mu\text{m}$) (d). The dotted line marks the zone of melting of all silumin phases.

Table 3. Thickness of the melting zone of the bare and ZrN-coated silumin after electron beam treatment.

Sample No.	1	2	3	4
Coating thickness h , μm	0	0.5 ± 0.08	1 ± 0.11	2 ± 0.14
Melting zone thickness after 5 pulses, μm (experiment)	33.8 ± 6.3	38.2 ± 7.9	45.4 ± 7.1	47.6 ± 8.3
Melting zone thickness after 1 pulse (calculation)	48	54	57	52

Typical waveforms of the recorded signals are shown in Figure 4. The pulsed current in the acceleration gap reached 100–120 A; its waveform had a rectangular shape with a width at half maximum of 150 μs and rise rate of about 10 A/ μs . The pulse power, measured in the acceleration gap circuit, varied non monotonically; after reaching a maximum (1.3–1.4 MW), it decreased due to discharging of the storage capacitor bank (Figure 4). In this case, the sample surface temperature continued to increase or remained approximately constant. The measured energy density delivered by the electron beam to the target in this mode was about 25 J/ cm^2 .

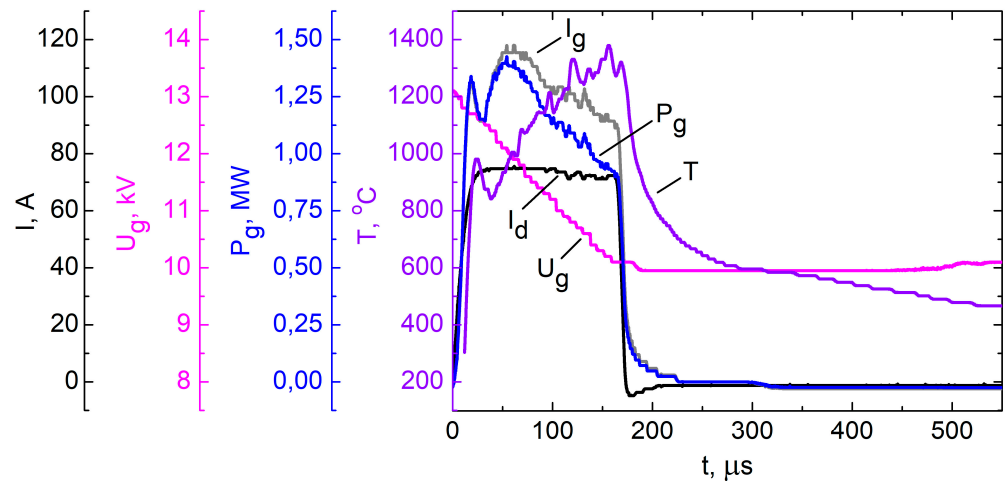


Figure 4. Waveforms of the plasma cathode discharge current I_d , current in the acceleration gap, I_g , accelerating voltage U_g , and surface temperature T , and time variations of the pulse power in the acceleration gap circuit, P_g for the sample with a 1- μm coating.

The experimental pulses of the electron beam power density for the bare silumin and the silumin with a coating of thickness 0.5, 1, and 2 μm , are shown in Figure 5. The average power density was $1.8 \times 10^5 \text{ W/cm}^2$. Figure 6 shows the sample surface temperature for the corresponding power density pulses (see Figure 5).

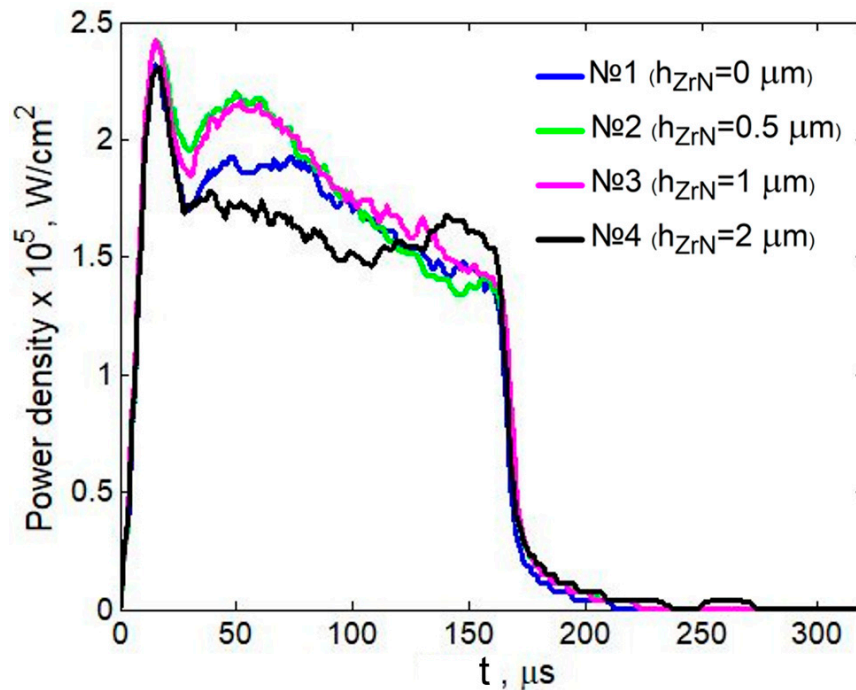


Figure 5. Time variations of the experimental power density during electron beam treatment for the bare and ZrN-coated silumin samples.

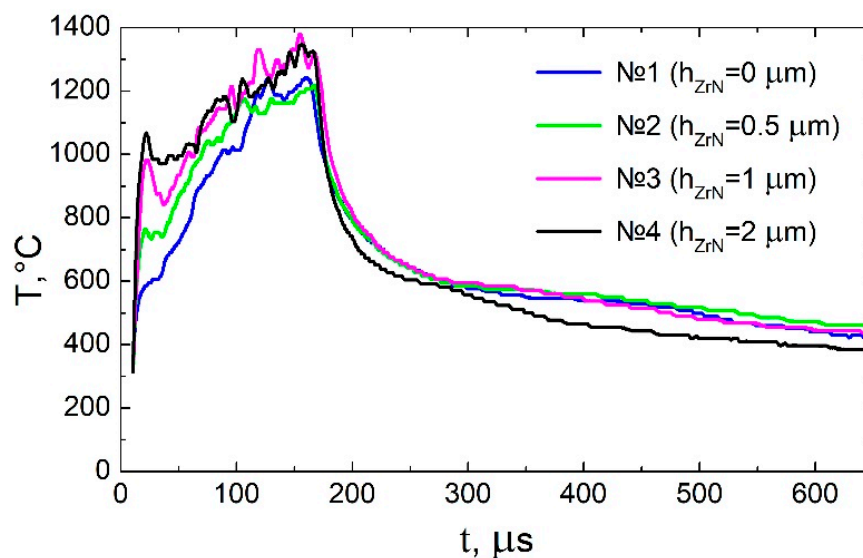


Figure 6. Time variations of the local surface temperature during electron beam treatment for the bare and ZrN-coated silumin samples.

As can be seen from the time variations of the sample surface temperature (see Figure 6), increasing the thickness of the ZrN coating substantially increased both the temperature rise rate and the maximum temperature reached during the rise time of the power density pulse (Table 4). Thus, when the coating thickness was increased from 0.5 to 2 μm , the rise rate of the surface temperature measured during the power density rise increased by a factor of 1.5 (from 6×10^7 to 9×10^7 K/s) and the peak temperature increases by 40% (from 760 to 1070 $^{\circ}\text{C}$).

Table 4. Surface temperature characteristics for the bare and ZrN-coated silumin samples subjected to pulsed electron beam treatment.

ZrN Coating Thickness, μm	0	0.5	1	2
Temperature rise rate during the pulse rise, deg/s	3×10^7	6×10^7	7×10^7	9×10^7
Maximum temperature during the pulse rise, $^{\circ}\text{C}$	605	760	980	1070
Maximum temperature in a pulse, $^{\circ}\text{C}$	1200	1220	1380	1350

Comparing the maximum temperature between the samples coated with 0.5- μm and 1- μm ZrN, it can be seen that it is 160 degrees higher for the latter (1380 $^{\circ}\text{C}$) than for the former (1220 $^{\circ}\text{C}$) (see Figure 6, Table 4). Note that the power density pulses in the acceleration gap for these cases differ insignificantly (see Figure 5). This indicates that the thickness of the coating affected the local temperature of the sample surface.

After the end of the beam current pulse, the surface temperature decreased exponentially, with an average rate of about 6×10^6 deg/s, to a phase transition temperature of 570–580 $^{\circ}\text{C}$, which was the same for all samples. For the sample with a coating of thickness 2 μm , the measured surface cooling rate was 1.3×10^7 deg/s (see Figure 6). For the other samples, it turned out to be slightly higher. When the surface temperature of the sample decreased below the crystallization temperature, it was observed to cool at a rate of $(5\text{--}6) \times 10^5$ deg/s.

The results of the numerical calculations are shown in Figures 7–11. The behavior of the surface temperature $T(t)$ of the bare and coated silumin calculated for the experimental power pulses (see Figure 5) is shown in Figure 7. The crystallization of the silumin melt depended on the thermophysical characteristics of the coating, and its rate decreased with an increase in coating thickness. This might be due to a decrease in the number of unmelted crystals, which acted as crystallization centers. The crystallization rate also depended

on the amount of energy deposited into the irradiated sample; the large amount of heat released during crystallization decreased its rate.

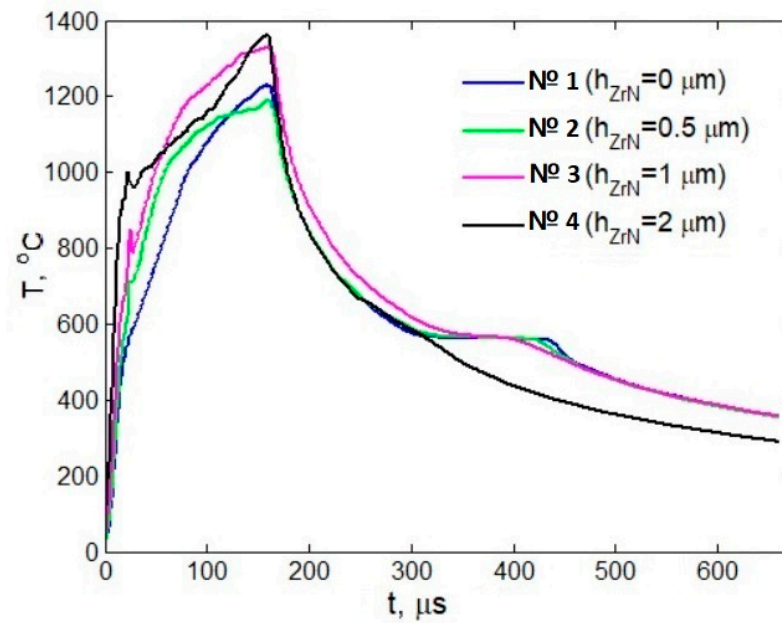


Figure 7. Time variations of the surface temperature of the bare and coated silumin during electron beam treatment.

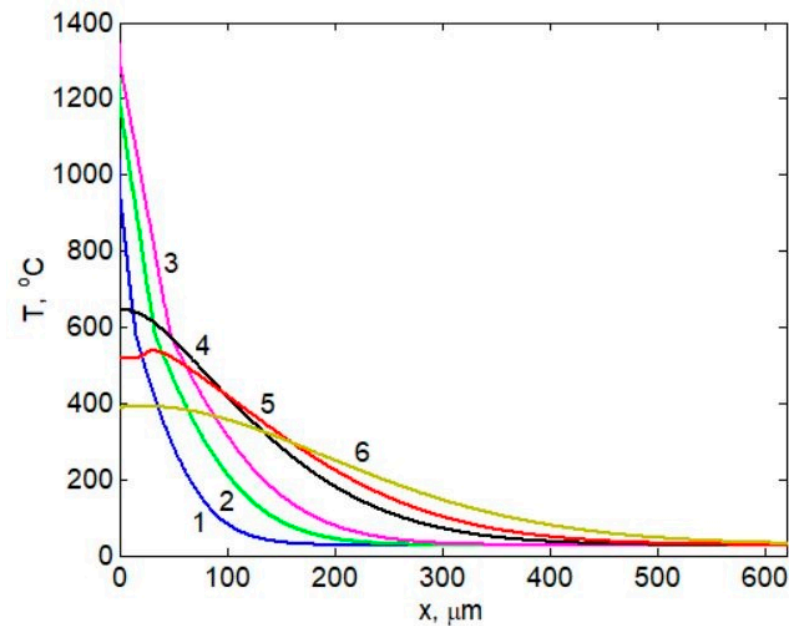


Figure 8. Temperature distribution in depth for the 1- μm coated silumin at different points of time during electron beam irradiation: 50 (curve 1), 100 (curve 2), 150 (curve 3), 300 (curve 4), 400 (curve 5), and 600 μs (curve 6).

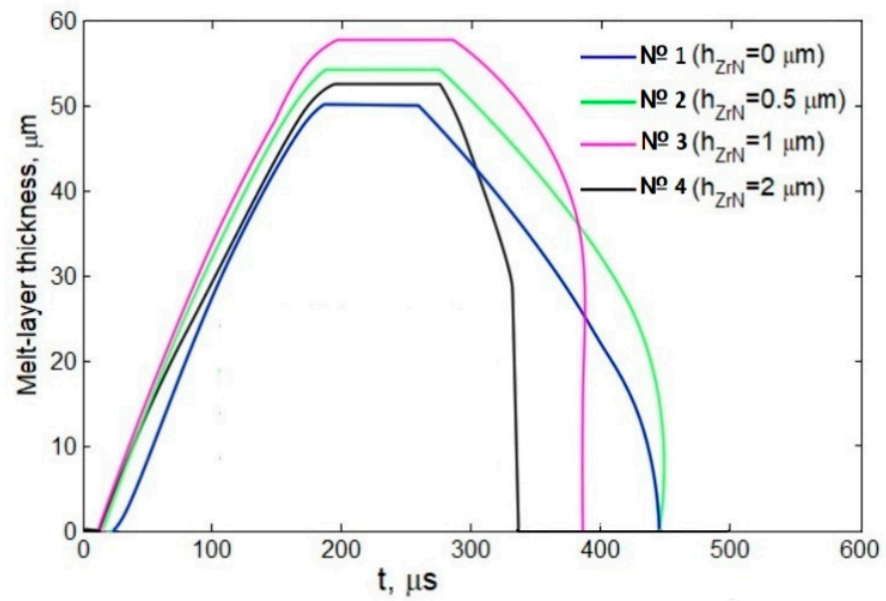


Figure 9. Time variations of the melt depth for the bare silumin sample and for the silumin samples with a coating of thickness 0.5, 1, and 2 μm .

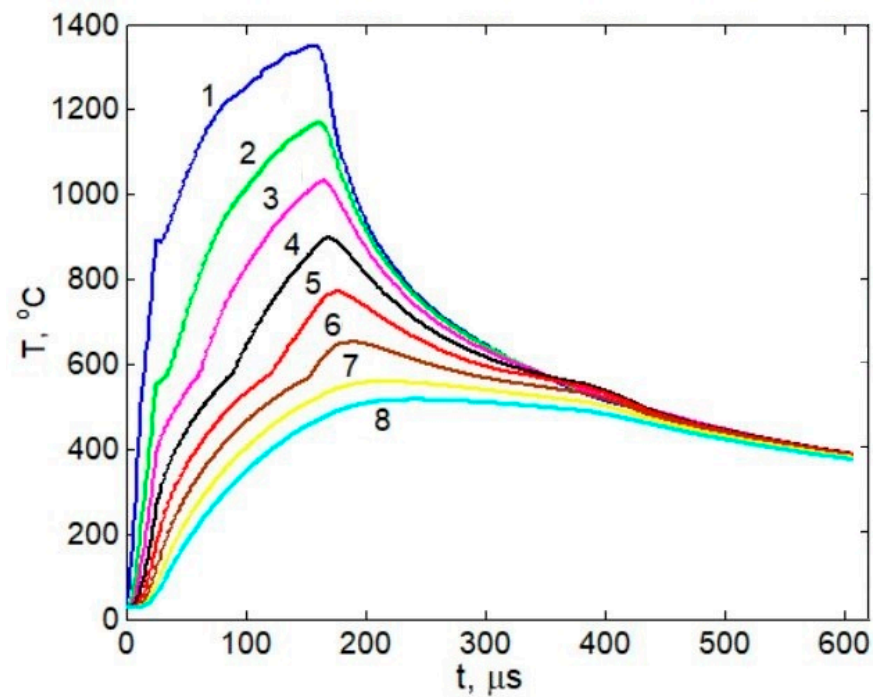


Figure 10. Time variations of the temperature at different depths of the silumin sample with a 1- μm coating: depth = 0 (curve 1), 10 (curve 2), 20 (curve 3), 30 (curve 4), 40 (curve 5), 50 (curve 6), 60 (curve 7), and 70 μm (curve 8).

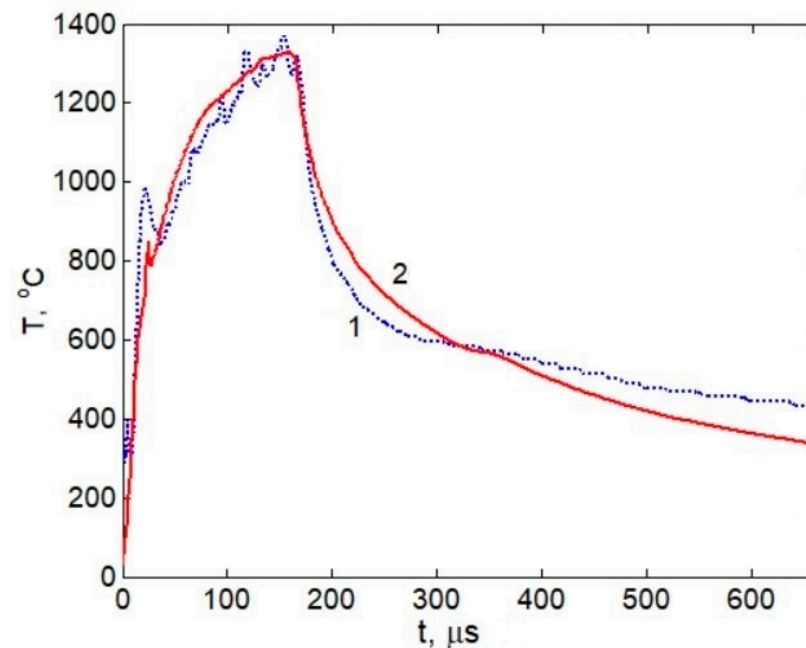


Figure 11. Time variations of the measured (curve 1) and calculated surface temperature (curve 2) for the silumin sample with a 1- μm coating.

The temperature fields in the bare and coated silumin samples varied in almost the same way. Figure 8 shows the temperature distribution in depth for the 1- μm coated silumin at different points of time during electron beam irradiation. The maximum temperature gradient in the melt zone was ~ 10 deg/ μm , while at the melt boundary it was 3.8 deg/ μm and remained unchanged for about 100 μs .

The numerical calculations have shown that a surface layer with a thickness of no more than 57 μm was melted in all samples subjected to electron beam irradiation. The difference between the experimental depth of the melt and the calculated one (see Table 3) might be associated with a change in the properties of the structure of the surface layer upon penetration of coating fragments into it after five irradiation pulses. Figure 9 shows the time variation in melt depth during electron beam irradiation for the bare silumin sample and for the silumin samples with a coating of thickness 0.5, 1, and 2 μm . The melt depth in the samples increased during the irradiation pulse at a rate of $\sim 3 \times 10^5$ $\mu\text{m}/\text{s}$. The irradiation was stopped in 150 μs , and the decrease in melt temperature determined by the thermal conductivity of the silumin due to the propagation of heat from the treatment zone into the bulk sample.

The melt depth remained unchanged within 300 μs , until the surface temperature reached the crystallization temperature of the silumin. The lifetime of the liquid phase in the samples with a 0.5- μm and a 2- μm coating was 450 and 350 μs , respectively.

Figure 10 shows how the temperature varied with time at different depths of the silumin sample with a 1- μm coating. The heating and cooling rates decreased with increasing distance from the surface. At a depth of more than 55 μm , the temperature was below the eutectic temperature (577 $^{\circ}\text{C}$). Thus, at a depth of 60 μm , a temperature of ~ 550 $^{\circ}\text{C}$ persisted for ~ 250 μs .

Figure 11 shows the time variations of the surface temperature $T(t)$ calculated and measured for the sample with a 1- μm coating. The variations in $T(t)$ correlate with the variations in the electron beam power density during the pulse (see Figure 5). The smaller fluctuations in the experimental curves of $T(t)$ can be explained by the sensitivity of the measuring device to a change in the emissivity caused by a change in the state of the sample surface during the pulse.

5. Conclusions

A eutectic silumin was subjected to a combined treatment, including the deposition of a ZrN coating on a silumin substrate and the treatment of the coating/substrate system with a pulsed electron beam of submillisecond duration. Examination of thin transverse sections of the ZrN-coated silumin performed after electron beam treatment revealed an extended melt zone, the thickness of which was 30–55 μm for all samples. In the melt zone of the samples with coatings of thickness 0.5–2 μm irradiated with five electron beam pulses, a partial immersion of the coating into the bulk substrate to a depth of 45 μm was observed.

Local measurements of the temperature in the electron beam treatment zone, numerical modeling of the fast heating (within 150 μs) and solidification of the melt under the action of an intense heat source were carried out for the action of experimental electron beam pulses ($1.8 \times 10^9 \text{ W/cm}^2$) on the bare and the ZrN-coated silumin. It was found that when the coating thickness was increased from 0.5 to 2 μm , the rise rate of the surface temperature increased from 6×10^7 to $9 \times 10^7 \text{ K/s}$ and the maximum temperature during the pulse rise increased from 760 to 1070 $^\circ\text{C}$. The melt depth was no more than 57 μm . The speed of the melt front during the pulse was $3 \times 10^5 \mu\text{m/s}$. The numerical simulation has shown that the eutectic temperature was not achieved at depths over 55 μm .

Comparing numerical calculations and measurements of the surface temperature of materials subjected to electron beam treatment, it is possible to elucidate the dynamics of the temperature field and melt depth in order to attain predetermined properties of materials upon electron beam treatment. It should be emphasized that the pulsed electron beam with unique parameters we used made it possible not only to trace in detail the dynamics of changes in the temperature of the molten surface layer of a ZrN-coated silumin sample, but also to produce a rather extended (tens of micrometers) modified structure. According to preliminary estimates, such a modified structure of the surface layer of a product made of silumin should significantly improve its operational properties. The results obtained are important for the development of technology for pulsed electron beam modification of the structure and surface properties of silumin products used in modern industry.

Author Contributions: Conceptualization, N.N.K., T.V.K. and O.V.K.; methodology, P.V.M., A.D.T. and Y.F.I.; formal analysis, O.V.K., P.V.M. and M.K.A.T.; investigation, O.V.K., E.A.P., P.V.M., A.D.T., M.K.A.T. and N.A.P.; data curation, O.V.K., N.N.K. and T.V.K.; writing—original draft preparation, O.V.K., P.V.M. and T.V.K.; writing—review and editing, N.N.K., T.V.K. and Y.F.I.; visualization, N.A.P. and E.A.P.; supervision, N.N.K. All authors have read and agreed to the published version of the manuscript.

Funding: This research was funded by the Ministry of Science and Higher Education of the Russian Federation (Grant No: FWRM-2021-0006).

Institutional Review Board Statement: Not applicable.

Informed Consent Statement: Not applicable.

Data Availability Statement: Not applicable.

Acknowledgments: The results of SEM were obtained at the Research and Education Centre “Physics and Chemistry of High-Energy Systems” of Tomsk State University.

Conflicts of Interest: The authors declare no conflict of interest.

References

1. Faye, D.N.; Dias, M.; Rojas-Hernandez, R.E.; Sousa, N.; Santos Luis, F.; Almeida Rui, M.; Alves, E. Structural and optical studies of aluminosilicate films doped with $(\text{Tb}^{3+}, \text{Er}^{3+})/\text{Yb}^{3+}$ by ion implantation. *Nucl. Inst. Methods Phys. Res. B* **2019**, *459*, 71–75. [[CrossRef](#)]
2. Kuang, X.; Lei, L.L.; Guodong, W.; Huang, L.K.; Xu, Y. The effect of N^+ ion-implantation on the corrosion resistance of HiPIMS-TiN coatings sealed by ALD-layers. *Surf. Coat. Technol.* **2019**, *374*, 72–82. [[CrossRef](#)]

3. Vorob'ev, V.L.; Gilmudinov, F.Z.; Bykov, P.V.; Bayankin, V.Y.; Pospelova, I.G.; Russkikh, I.T. Nanoscale layers formed on the surface of a titanium alloy by the ion-beam mixing of carbon with a substrate. *J. Synch. Investig.* **2019**, *13*, 979–984. [[CrossRef](#)]
4. Boes, J.; Röttger, A.; Becker, L.; Theisen, W. Processing of gas-nitrided AISI 316L steel powder by laser powder bed fusion—Microstructure and properties. *Addit. Manuf.* **2019**, *30*, 100836. [[CrossRef](#)]
5. Ren, Z.; Eppell, S.; Collins, S.; Ernst, F. Co–Cr–Mo alloys: Improved wear resistance through low-temperature gas-phase nitro-carburization. *Surf. Coat. Technol.* **2019**, *378*, 124943. [[CrossRef](#)]
6. Boblyyov, E. Diffusion saturation from fusible liquid metal media solutions by titanium of TK and WC-Co alloys as way to increase of tool durability. *IOP Conf. Ser. Mater. Sci. Eng.* **2018**, *453*, 032019. [[CrossRef](#)]
7. Sokolov, A.G.; Boblyyov, E.E. Diffusion saturation by titanium from liquid-metal media as way to increase carbide-tipped tool life. *Solid State Phenom.* **2017**, *265*, 181–186. [[CrossRef](#)]
8. Sridharan, N.; Isheim, D.; Seidman, D.N.; Babu, S.S. Colossal super saturation of oxygen at the iron-aluminum interfaces fabricated using solid state welding. *Scr. Mater.* **2017**, *130*, 196–199. [[CrossRef](#)]
9. Barda, H.; Rabkin, E. The role of interface diffusion in solid state dewetting of thin films: The nano-marker experiment. *Acta Mater.* **2019**, *177*, 121–130. [[CrossRef](#)]
10. *Metal Science and Heat Treatment of Metals*; Lakhtin, Y.M. (Ed.) Mashgiz: Moscow, Russia, 1955. (In Russian)
11. Romanov, D.A.; Gromov, V.E.; Budovskikh, E.A.; Ivanov, Y.F. Regularities of formation of structural-phase states on a surface of metals and alloys at an electroexplosive alloying. *Usp. Fiz. Met.* **2015**, *16*, 119–157. [[CrossRef](#)]
12. Zagulyaev, D.V.; Gromov, V.E.; Ivanov, Y.F.; Petrikova, E.A.; Teresov, A.D.; Konvalov, S.V.; Semin, A.P. Study of the surface relief, structure and phase composition of the silumin composite layer obtained by the method of electric explosion alloying by Al-Y₂O₃ system. *J. Phys. Conf. Ser.* **2018**, *1115*, 032021. [[CrossRef](#)]
13. Romanov, D.; Sosnin, K.; Pronin, S.; Konvalov, S.; Moskovskii, S.; Gromov, V.; Ivanov, Y.; Bataev, V.; Semin, A. Electroexplosive hafnium coating on titanium implant modified by nitrogen ions and electron beam processing. *Surf. Coat. Technol.* **2021**, *409*, 126895. [[CrossRef](#)]
14. Ivanov, Y.F.; Gromov, V.E.; Romanov, D.A.; Ivanova, O.V.; Rubannikova, Y.A. Surface boriding and titanization stainless steel by integrated processes. *J. Surf. Investig. X-Ray Synchrotron Neutron Tech.* **2021**, *15*, 200–209. [[CrossRef](#)]
15. Ivanov, Y.F.; Gromov, V.E.; Romanov, D.A.; Ivanova, O.V.; Teresov, A.D. Liquid-phase boriding of high-chromium steel. *Steel Transl.* **2020**, *50*, 452–459. [[CrossRef](#)]
16. Cherenda, N.N.; Shymanski, V.I.; Uglov, V.V.; Astashinskii, V.M.; Kuz'mitskii, A.M.; Koval, N.N.; Ivanov, Y.F.; Teresov, A.D. Formation of zirconium–titanium solid solutions under the action of compression plasma flows and high-current electron beams. *Inorg. Mater. Appl. Res.* **2012**, *3*, 365–370. [[CrossRef](#)]
17. Uglov, V.V.; Kudaktin, R.S.; Petukhou, Y.A.; Kvasov, N.T.; Punko, A.V.; Astashynski, V.M. Mass transfer in “metal layer–silicon substrate” systems under the action of compression plasma flows. *Appl. Surf. Sci.* **2012**, *258*, 7377–7383. [[CrossRef](#)]
18. Uglov, V.V.; Sari, A.H.; Astashynski, V.M.; Kuzmitski, A.M.; Petukhov, Y.A. Phase transformations in Ta-Si system induced by compression plasma flow. *Eur. Phys. J. Appl. Phys.* **2014**, *65*, 10801. [[CrossRef](#)]
19. Shymanski, V.I.; Cherenda, N.N.; Uglov, V.V.; Astashynski, V.M.; Kuzmitski, A.M. Structure and phase composition of Nb/Ti system subjected to compression plasma flows impact. *Surf. Coat. Technol.* **2015**, *278*, 183–189. [[CrossRef](#)]
20. Rotshtein, V.P.; Kolubaeva, Y.A.; Mei, X.; Markov, A.B.; Naiden, E.P.; Oskomov, K.V.; Pryadko, E.L.; Teresov, A.D.; Shulepov, I.A.; Shulov, V.A. Effect of conditions of pulsed electron-beam melting for Al (film)/Ti (substrate) systems on phase formation and properties of Ti-Al surface alloys. *Tech. Phys. Lett.* **2012**, *38*, 780–783. [[CrossRef](#)]
21. Markov, A.B.; Yakovlev, E.V.; Shepel', D.A.; Petrov, V.I.; Bestetti, M. Liquid-phase surface alloying of copper with stainless steel using low-energy, high-current electron beam. *Russ. Phys. J.* **2017**, *60*, 1455–1460. [[CrossRef](#)]
22. Rotshtein, V.P.; Ivanov, Y.F.; Kolubaeva, Y.A.; Mei, X.; Markov, A.B.; Naiden, E.P.; Ozur, G.E.; Oskomov, K.V.; Popov, S.A.; Pryadko, E.L.; et al. Synthesis of Ti₃Al and TiAl based surface alloys by pulsed electron-beam melting of Al(film)/Ti(substrate) system. *Tech. Phys. Lett.* **2011**, *37*, 226–229. [[CrossRef](#)]
23. Markov, A.B.; Mikov, A.V.; Ozur, G.E.; Padei, A.G. A PITM-CPI facility for the surface alloying. *Instrum. Exp. Tech.* **2011**, *54*, 862–866. [[CrossRef](#)]
24. Ivanov, Y.F.; Petrikova, E.A.; Ivanova, O.V.; Ikonnikova, I.A.; Teresov, A.D.; Shugurov, V.V.; Krysin, O.V. Modification of a coating (TiN)—substrate (VT1-0) system with high-intensity pulsed electron beams. *Russ. Phys. J.* **2015**, *58*, 366–372. [[CrossRef](#)]
25. Ivanov, Y.F.; Petrikova, E.A.; Ivanova, O.V.; Ikonnikova, I.A.; Teresov, A.D.; Shugurov, V.V.; Krysin, O.V. Structure and properties of a coating (TiCuN)—substrate (A7) system modified with a high-intensity electron beam. *Russ. Phys. J.* **2015**, *58*, 373–379. [[CrossRef](#)]
26. Zolotarevsky, V.S.; Belov, N.A.; Glazoff, M.V. *Casting Aluminium Alloys*; Elsevier: Amsterdam, The Netherlands, 2007; 530p. [[CrossRef](#)]
27. Belov, N.A.; Savchenko, S.V.; Khvan, A.V. *Phase Composition and Structure of Silumins*; MISIS: Moscow, Russia, 2008. Available online: https://rusneb.ru/catalog/000199_000009_003419627/ (accessed on 24 November 2021). (In Russian)
28. Brandt, R.; Bender, W.; Grün, G.U.; Neuer, G. Thermal Conductivity of Ternary and Multi-Component Aluminum Alloys up to and above the Melting Temperature. In *Continuous Casting: Proceedings of the International Conference on Continuous Casting of Non-Ferrous Metals*; John Wiley & Sons: Hoboken, NJ, USA, 2006; pp. 174–181. [[CrossRef](#)]

29. Grigo'ev, I.S.; Meilikhov, E.Z. *Handbook of Physical Values*; Energoatomizdat: Moscow, Russia, 1991. Available online: [https://www.scirp.org/\(S\(czeh2tfqyw2orz553k1w0r45\)\)/reference/ReferencesPapers.aspx?ReferenceID=1378729](https://www.scirp.org/(S(czeh2tfqyw2orz553k1w0r45))/reference/ReferencesPapers.aspx?ReferenceID=1378729) (accessed on 24 November 2021).
30. Sarychev, V.; Nevskii, S.; Konovalov, S.; Granovskii, A.; Ivanov, Y.; Gromov, V. Model of nanostructure formation in Al–Si alloy at electron beam treatment. *Mater. Res. Express* **2019**, *6*, 026540. [[CrossRef](#)]
31. Harrison, R.W.; Lee, W.E. Processing and properties of ZrC, ZrN and ZrCN ceramics: A review. *Adv. Appl. Ceram.* **2016**, *115*, 294–307. [[CrossRef](#)]
32. Shugurov, V.V.; Koval, N.N.; Krysin, O.V.; Prokopenko, N.A. QUINTA equipment for ion-plasma modification of materials and products surface and vacuum arc plasma-assisted deposition of coatings. *J. Phys. Conf. Ser.* **2019**, *1393*, 012131. [[CrossRef](#)]
33. Krysin, O.V.; Ivanov, Y.F.; Prokopenko, N.A.; Shugurov, V.V.; Petrikova, E.A.; Denisova, Y.A.; Tolkachev, O.S. Influence of Nb addition on the structure, composition and properties of single-layered ZrN-based coatings obtained by vacuum-arc deposition method. *Surf. Coat. Technol.* **2020**, *387*, 125555. [[CrossRef](#)]
34. Devyatkov, V.N.; Koval, N.N.; Grigoriev, S.V.; Teresov, A.D. Equipment for pulsed thermal treatment of the surfaces of materials by a low-energy electron beam. *High Temp. Mater. Process.* **2013**, *17*, 187–194. [[CrossRef](#)]
35. Akhmadeev, Y.H.; Grigoriev, S.V.; Koval, N.N.; Schanin, P.M. Plasma sources based on a low-pressure arc discharge. *Laser Part. Beams* **2003**, *21*, 249–254. [[CrossRef](#)]
36. Koval, N.N.; Grigoryev, S.V.; Devyatkov, V.N.; Teresov, A.D.; Schanin, P.M. Effect of intensified emission during the generation of a submillisecond low-energy electron beam in a plasma-cathode diode. *IEEE Trans. Plasma Sci.* **2009**, *37*, 1890. [[CrossRef](#)]
37. Chen, S.H.; Cho, D.H.; Kocamustafaogullary, G. Melting and solidification with internal radiative transfer—A generalized phase change model. *Intern. J. Heat Mass Transfer.* **1983**, *26*, 621–633. [[CrossRef](#)]
38. Comsol Multiphysics, Heat Transfer Module User's Guide, Version 5.0. p. 173. Available online: <https://doc.comsol.com/5.4/doc/com.comsol.help.heat/HeatTransferModuleUsersGuide.pdf> (accessed on 24 November 2021).
39. Teresov, A.D.; Koval, T.V.; An, T.M.K.; Moskvina, P.V. Experimental and numerical study of the impact of a pulsed electron beam on titanium and aluminum targets. *Bull. Russ. Acad. Sci. Phys.* **2019**, *83*, 1397–1401. [[CrossRef](#)]
40. Vorobyov, M.; Koval, T.; Shin, V.; Moskvina, P.; An, T.M.K.; Koval, N.; Ashurova, K.; Doroshkevich, S.; Torba, M. Controlling the Specimen surface temperature during irradiation with a submillisecond electron beam produced by a plasma-cathode electron source. *IEEE Trans. Plasma Sci.* **2021**, *49*, 2550–2553. [[CrossRef](#)]